

Fig. 4. GFP-labeled mitochondria are shown in the body wall muscle cells of L4 animals of the following genotypes: (A) wild-type N2, (B) *anc-1(e1873)*, (C) *unc-84(n369)*, and (D) cofilin *unc-60(r398)*. The severely abnormal mitochondria in *anc-1(e1873)* are not anchored. In live animals, they were seen moving throughout the muscle as the animal moved. Scale bar, 10 μ m.

and spread throughout the cell as the worm moved. In contrast, mitochondria in *anc-1(e1873)* animals were spherically shaped, often clustered together, and were pushed around within the cytoplasm as the animal moved (Fig. 4B). Mitochondria were not shaped or positioned properly in an *unc-60(r398)* mutant background (Fig. 4D). A partial loss-of-function allele in the *C. elegans* cofilin homolog, *unc-60(r398)*, disrupts actin filaments in the body wall muscle of adult hermaphrodites (23). Therefore, actin filaments are required for proper positioning of mitochondria. The anchorage of mitochondria in *unc-84(n369)* was normal (Fig. 4C), suggesting that ANC-1 does not require UNC-84 to anchor mitochondria as it does for nuclear anchorage.

Our model (fig. S4) suggests that ANC-1 functions to anchor nuclei by tethering the nucleus to the actin cytoskeleton and predicts that the KASH domain of ANC-1 is localized to the outer nuclear envelope by UNC-84. Digitonin extraction experiments show that human Syne-2 localizes to the outer nuclear envelope (14). ANC-1 would then extend away from the nucleus, where its NH₂-terminus binds to the stable actin cytoskeleton. As a result, ANC-1 molecules function to directly attach the actin cytoskeleton to the nuclear envelope. Before a nucleus can migrate through the cytoplasm of the cell, the nuclear anchor must be released. The SUN domain of UNC-84 is likely to be intimately involved with this switch in nuclear behavior, because it is required for both ANC-1 and UNC-83 localization at the nuclear envelope (21) (Fig. 2). UNC-83 is required for normal nuclear migration but not for nuclear anchorage (21). It is not known whether ANC-1 and UNC-83 can interact with UNC-84 simultaneously, although both antigens are detected at the nuclear envelope of adult hypodermal cells. Overexpression of UNC-83 did not cause any obvious anchorage phenotype, eliminating a competition model.

Dystrophin and the associated dystrophin-glycoprotein complex function to connect the actin cytoskeleton to the extracellular matrix; mutations in these components lead to Duchenne or Becker muscular dystrophies (24). Although ANC-1 and Syne connect the

actin cytoskeleton to the nuclear matrix whereas dystrophin connects actin to the extracellular matrix, there are some similarities between these two mechanisms. ANC-1 and associated proteins, including UNC-84 and lamin A/C (12), are likely to create a bridge across the nuclear envelope. Mutations in the gene encoding lamin A/C lead to Emery-Dreifuss muscular dystrophy (24), which suggests a potential link between the ANC-1 and Syne proteins and muscular dystrophy.

References and Notes

1. N. R. Morris, *J. Cell Biol.* **148**, 1097 (2000).
2. S. Reinsch, P. Gonczyk, *J. Cell Sci.* **111**, 2283 (1998).
3. G. M. Guild, P. S. Connelly, M. K. Shaw, L. G. Tilney, *J. Cell Biol.* **138**, 783 (1997).
4. E. Chytilova *et al.*, *Mol. Biol. Cell* **11**, 2733 (2000).
5. J. E. Sulston, H. R. Horvitz, *Dev. Biol.* **56**, 110 (1977).
6. C. J. Malone, W. D. Fixsen, H. R. Horvitz, M. Han, *Development* **126**, 3171 (1999).

7. E. M. Hedgecock, J. N. Thomson, *Cell* **30**, 321 (1982).
8. Materials and methods are available as supporting material on Science Online.
9. K. L. Mosley-Bishop, Q. Li, L. Patterson, J. A. Fischer, *Curr. Biol.* **9**, 1211 (1999).
10. M. A. Welte, S. P. Gross, M. Postner, S. M. Block, E. F. Wieschaus, *Cell* **92**, 547 (1998).
11. E. D. Apel, R. M. Lewis, R. M. Grady, J. R. Sanes, *J. Biol. Chem.* **275**, 31986 (2000).
12. J. M. Mislow, M. S. Kim, D. B. Davis, E. M. McNally, *J. Cell Sci.* **115**, 61 (2002).
13. Q. Zhang *et al.*, *J. Cell Sci.* **114**, 4485 (2001).
14. Y. Y. Zhen, T. Libotte, M. Munck, A. A. Noegel, E. Korenbaum, *J. Cell Sci.* **115**, 3207 (2002).
15. Y. Rosenberg-Hasson, M. Renert-Pasca, T. Volk, *Mech. Dev.* **60**, 83 (1996).
16. T. Volk, *Development* **116**, 721 (1992).
17. Y. Yan *et al.*, *Science* **262**, 2027 (1993).
18. M. Gimona, K. Djinnovic-Carugo, W. J. Kranewitter, S. J. Winder, *FEBS Lett.* **513**, 98 (2002).
19. H. R. Horvitz, J. E. Sulston, *Genetics* **96**, 435 (1980).
20. K. K. Lee *et al.*, *Mol. Biol. Cell* **13**, 892 (2002).
21. D. A. Starr *et al.*, *Development* **128**, 5039 (2001).
22. A. Fire *et al.*, *Nature* **391**, 806 (1998).
23. S. Ono, D. L. Baillie, G. M. Benian, *J. Cell Biol.* **145**, 491 (1999).
24. E. A. Burton, K. E. Davies, *Cell* **108**, 5 (2002).
25. We thank Han lab members and L. Chen for their advice; S. McCauley, G. Ackerman, and L. Chlipala for technical assistance; and the *Caenorhabditis* Genetics Center, J. Hodgkin, S. Ono, P. Mains, A. Fire, A. Coulson, and Y. Kohara for materials. Supported by NIH and Howard Hughes Medical Institute.

Supporting Online Material

www.sciencemag.org/cgi/content/full/1075119/DC1
Materials and Methods
Supporting Text
Figs. S1 to S4
References and Notes

17 June 2002; accepted 29 July 2002
Published online 8 August 2002;
10.1126/science.1075119
Include this information when citing this paper.

Neural Correlates for Perception of 3D Surface Orientation from Texture Gradient

Ken-Ichiro Tsutsui,^{1*} Hideo Sakata,^{1,2} Tomoka Naganuma,^{1,3} Masato Taira^{1†}

A goal in visual neuroscience is to reveal how the visual system reconstructs the three-dimensional (3D) representation of the world from two-dimensional retinal images. Although the importance of texture gradient cues in the process of 3D vision has been pointed out, most studies concentrate on the neural process based on binocular disparity. We report the neural correlates of depth perception from texture gradient in the cortex. In the caudal part of the lateral bank of intraparietal sulcus, many neurons were selective to 3D surface orientation defined by texture gradient, and their response was invariant over different types of texture pattern. Most of these neurons were also sensitive to a disparity gradient, suggesting that they integrate texture and disparity gradient signals to construct a generalized representation of 3D surface orientation.

The real world is three-dimensional (3D), but when projected to the retina it is reduced to a two-dimensional (2D) image. Nevertheless, what we see and what we perceive is all 3D. Therefore, the brain must be reconstructing the 3D representation of the real world from the 2D images on the retinae. Among many

kinds of depth cues, binocular disparity has been suggested to be critical in many psychophysical studies (1–3). Neurons in striate (4–7) and extrastriate (6–10) visual areas are sensitive to binocular disparity signals. Recently, neurons that code 3D features of a visual surface by higher-order processing of

REPORTS

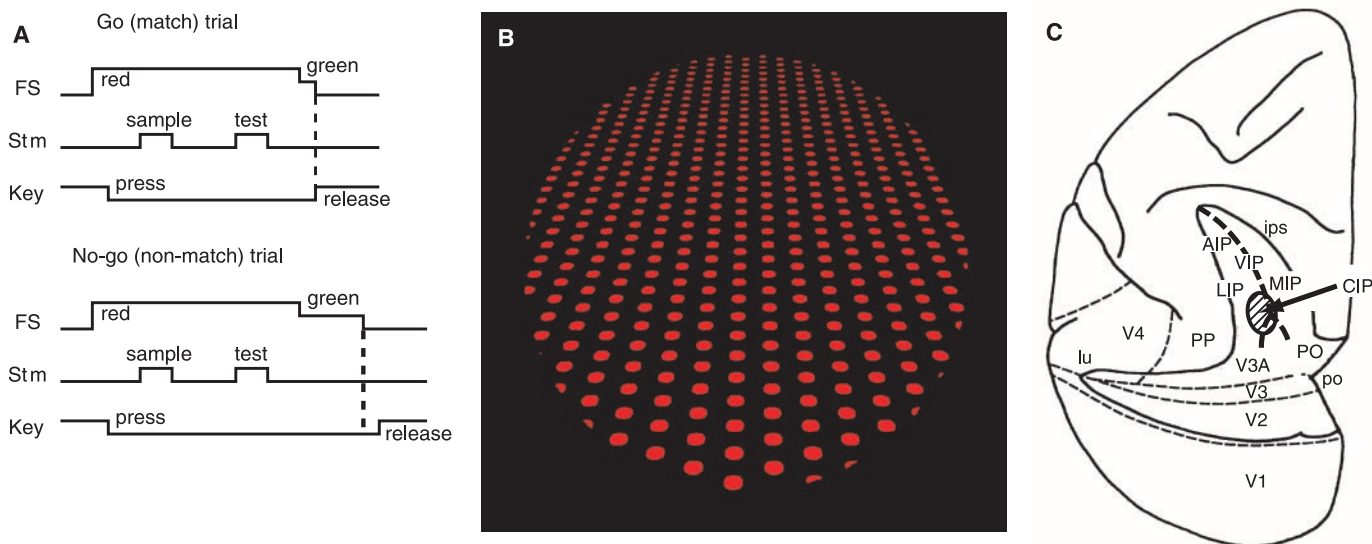


Fig. 1. (A) Time course of delayed match-to-sample task. To obtain a reward, monkeys had to discriminate the orientation of the sample and test stimuli and make a go or no-go response depending on whether the surface orientations of the sample and test stimuli were the same or different. Duration of stimulus presentation was about 1 s, and that of delay between sample and test stimulus presentations was about 2 s. When the test stimulus matched the sample, monkeys had to make a go response; when the test stimulus did not match the sample, they had to make a no-go response. FS = fixation spot. **(B)** Texture pattern with dot

elements (dot-TP). Surface orientation of backward inclination (270° tilt) is defined by texture gradient of dot elements. By rotating the figure counterclockwise around the z axis, the surface orientation varies as right side nearer (0° tilt), forward (90° tilt), and left side nearer (180° tilt). Dot-TP had texture spacing cues and texture element size and shape cues for 3D orientation. Line-TP had perspective cues as well as texture spacing cues. **(C)** Schematic indicating the location of CIP. The intraparietal sulcus (ips), lunette sulcus (lu), and parietooccipital sulcus (po) are unfolded. CIP is located between areas LIP and V3A.

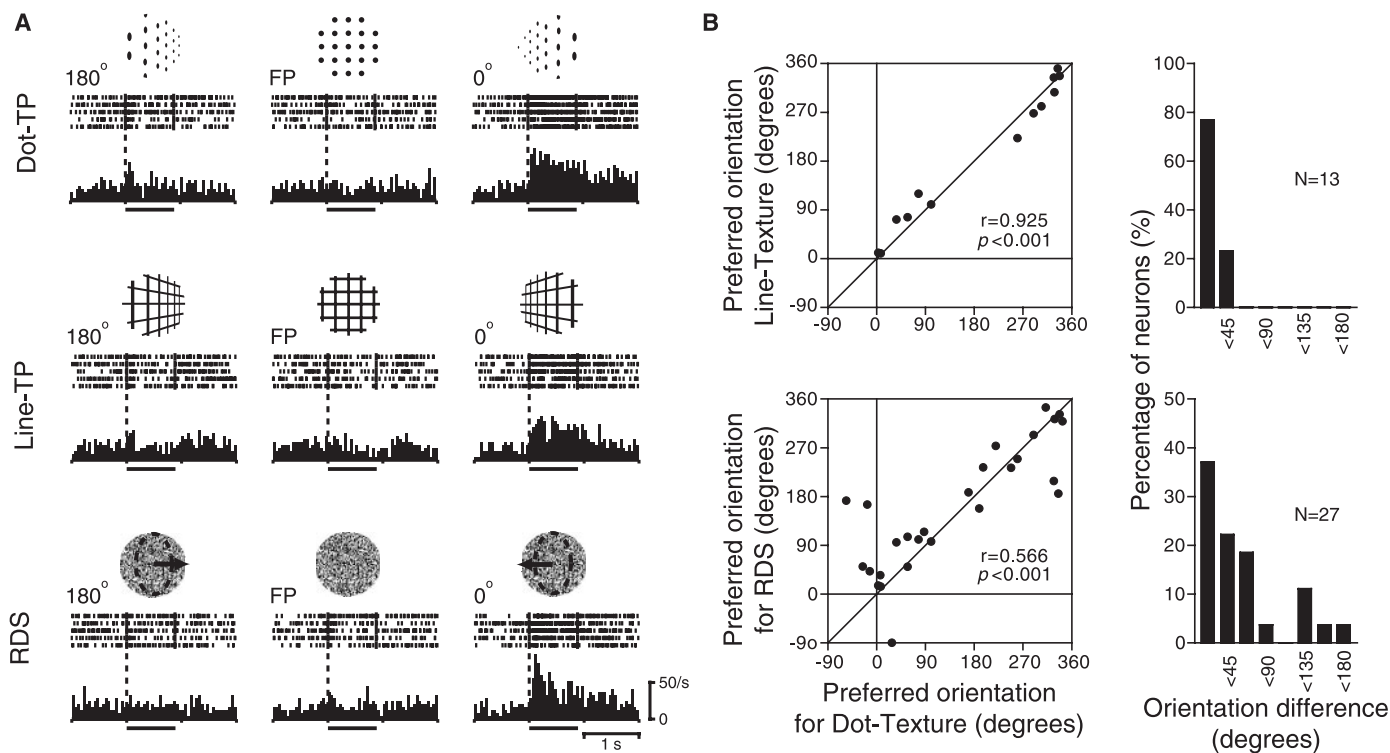


Fig. 2. (A) Responses of a texture gradient-sensitive neuron (22) to dot-TP (top row), line-TP (middle row), and RDS (bottom row) aligned at the onset of sample stimulus presentation. Responses to three orientations are shown, although responses to nine orientations were recorded. Bars below histograms indicate stimulus presentation duration. Insets above rasters indicate stimuli presented: dashed lines and arrows in RDS schematically represent the surface orientation and surface normal

caused by binocular disparity, respectively. Numbers at the top left of rasters indicate tilt angle. FP indicates frontoparallel orientation. **(B)** Scatter plots of preferred orientations with different types of stimulus (left column) and distribution histograms of the preferred orientation difference (right column). Data for dot-TP versus line-TP are shown in the top row, and those for dot-TP versus RDS are shown in the bottom row. In scatter plots, each dot represents an individual neuron.

REPORTS

disparity signals have been found in the parietal (11, 12) and temporal (13, 14) association cortices. However, binocular disparity is not the only cue for depth perception, because we can perceive depth even with one eye closed. Gibson (15) has proposed that texture gradient is an important cue for depth perception comparable to binocular disparity. This hypothesis has been supported by psychophysical (16) and computational (17) studies. However, there have been few neurophysiological data concerning the neural correlates for the perception of depth from texture gradient cues (18). The purpose of this study was to examine how texture gradient cues are processed to reconstruct 3D representations of visual stimuli.

We trained two male monkeys (*Macaca fuscata*) to perform a delayed-match-to-sample (Fig. 1A) of 3D surface orientation by using the stimulus sets of texture pattern without disparity (Fig. 1B) and a random-dot stereogram (RDS) independently (19). During task performance, we recorded single-unit activities in the caudal part of the lateral bank of intraparietal sulcus (Fig. 1C, area CIP), where we previously had found a group of neurons selective to a 3D surface orientation of a flat surface defined by binocular disparity (11, 12, 20, 21). We recorded 50 neurons during performance of the matching task with texture patterns (TPs) with dot elements (dot-TPs); 70% (35/50) of them showed selective response to a texture gradient of dot-TPs. Figure 2A shows the activity of a texture gradient-sensitive neuron (22). This neuron showed selective response to the texture gradient of dot-TP defining 0° tilt, or right-side-nearer orientation (top row). When this neuron was further tested with another set of texture patterns, TP with line elements (line-TP), it again showed selectivity to 0° tilt (middle row). As shown in this example, 81% (13/16) of the texture gradient-sensitive neurons tested with additional line-TPs responded selectively. In these neurons, orientation selectivity was highly correlated ($r = 0.925$; $P < 0.001$) between line-TP and dot-TP (Fig. 2B, top row). The difference of preferred orientation between two conditions was $<45^\circ$ in all these neurons. Therefore, texture gradient-sensitive neurons were not responding to the local feature of texture patterns per se but were specifically responding to the gradient signals extracted from the texture patterns. The representative neuron also responded to RDSs

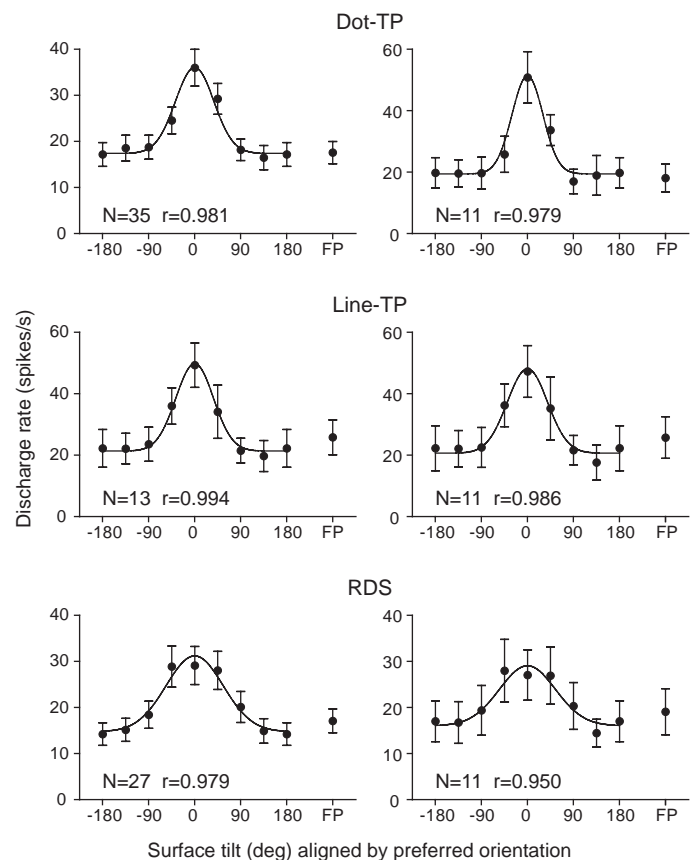
and again showed selectivity to the disparity gradient defining 0° tilt (Fig. 2A, bottom row). Similar to this neuron, 77% (27/35) of texture gradient-sensitive neurons showed selectivity to a 3D surface orientation defined by disparity gradients of RDS. In these neurons, orientation selectivity was significantly correlated ($r = 0.566$; $P < 0.001$) between dot-TP and RDS (Fig. 2B, bottom row). Distribution of the difference of preferred orientation between two conditions was highly concentrated to $<45^\circ$ (chi-square test; $P < 0.001$). These neurons may integrate texture and disparity gradient signals to construct a generalized representation of a 3D surface orientation.

The graphs in Fig. 3 show the average responses of neurons selective to the surface orientation of dot-TP, line-TP, and RDS. For each type of stimulus set, the Gaussian curve could be fitted to average responses to eight orientations with high regression coefficients. To compare the tuning sharpness for each stimulus set, the angular deviation S , which corresponds to the standard deviation in the normal distribution, was calculated and averaged over neurons. The mean S values of all dot-TP-, line-TP-, and RDS-selective neurons were 71.3, 70.0, and 69.3, respectively, and those of 11 neurons that were selective to all types of stimuli were 68.7, 69.4, and 73.0, respectively. The averaged S values did not differ significantly among different types of stimuli in either case (Student's t test; $P >$

0.10). Thus, the neural coding of surface orientation based on texture gradient was as precise as that based on disparity gradient in CIP neurons.

After the unit recording, we conducted a behavioral test to confirm that monkeys perceive depth from texture gradient. Although psychophysical studies suggest that humans perceive depth from texture gradient (15–17), there are few data to suggest that animals, including monkeys, perceive depth from texture gradient as humans do. This behavioral control is important, because texture gradient is a somewhat more ambiguous cue for depth than binocular disparity. Texture per se cannot be a cue for depth; it can be a cue for depth only after its gradients have been detected. We trained monkeys to cross-match the surface orientations defined by texture and disparity gradients by using TPs without any disparity as sample stimuli and RDSs as test stimuli (19). Figure 4 shows the success rate in the learning and test sessions of the cross-matching of two monkeys. In the learning sessions, the performance improved gradually and reached a $>80\%$ success rate after extensive training. In the test sessions, the monkeys performed the task with a success rate significantly higher than the chance level even in the first block and showed immediate progress of performance up to a $>80\%$ success rate in the following blocks.

Fig. 3. Average responses to nine orientations of neurons selective to the surface orientation of dot-TP (top), line-TP (middle), and RDS (bottom). Data averaged across all neurons available for a given stimulus type are shown in the left column, and those averaged across 11 neurons that displayed surface orientation selectivity in all three stimulus types are shown in the right column. In calculating the average response, we averaged the activity of each neuron with orientation of the strongest response realigned as 0° tilt separately for each stimulus type. FP on the abscissa indicates frontoparallel orientation. Error bars indicate SE. Gaussian curve was fitted to the graphs with high regression coefficients ($r > 0.95$ and goodness of fit $P > 0.99$ for every graph).

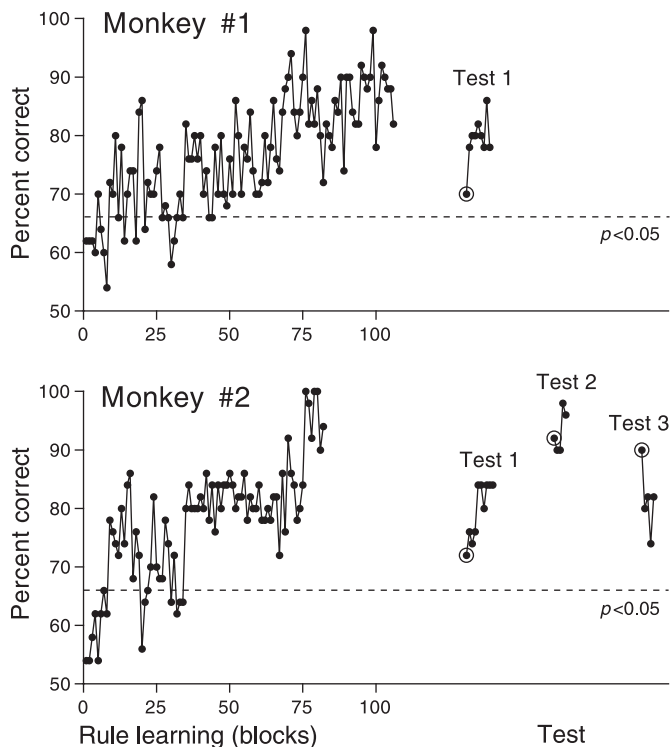


¹Department of Physiology and ²Department of Neurology, Nihon University School of Medicine, Tokyo 173-8610, Japan. ³Laboratory for Anatomy and Physiology, Seitoku Junior College of Nutrition, Tokyo 124-8530, Japan.

*Present address: Department of Anatomy, University of Cambridge, Cambridge CB2 3DY, UK.

†To whom correspondence should be addressed. E-mail: masato@med.nihon-u.ac.jp

Fig. 4. Learning curve for cross-matching of TP and RDS by two monkeys. Each dot represents success rate in a block of 50 trials. Dotted lines indicate the limit of success rates above the chance level (chi-square test; $P < 0.05$) for one block. Concentric circles indicate the first block of each test session. In these test sessions, success and error trials were all reinforced to examine monkeys' performance in the absence of correct/error feedback. Note that after the learning session, the monkeys could perform the task with a success rate above the chance level even in the first block of each test session. Monkey 2 performed better in the test session with diagonal orientations (test 2) than in those with oblique orientations (tests 1 and 3), suggesting that the transfer of learning depended more on surface orientation than on texture pattern.



After learning the task rule, the monkeys could thus correctly perform the cross-matching of texture and disparity gradients even with novel orientations (tests 1 and 3) and patterns (tests 2 and 3) without training. Monkeys regarded texture and disparity gradients as equivalent depth cues, and they perceived a 3D surface orientation from texture gradient cues.

We found that texture gradient is an important cue for perceiving a 3D surface orientation for monkeys as well as humans and that neurons in CIP play a critical role in perceiving a 3D surface orientation from texture gradient. This may be the first single-unit level demonstration of the neural basis of the 3D visual perception based on texture gradient, as suggested by Gibson (15). As a neural correlate of 3D vision based on monocular pictorial cues, we have already found that some surface orientation-selective neurons in CIP show sensitivity to linear perspective (12). However, this sensitivity was relatively weak, which may be due to the ambiguity of the linear perspective cues used in the experiment. We also found in this study that most texture gradient-sensitive neurons in CIP were sensitive to disparity gradient (23) and that the preferences of each neuron for texture and disparity gradients were almost the same in terms of surface tilt, suggesting that they integrate texture and disparity gradient signals to construct a generalized

representation of 3D surface orientation. Thus, we assume that CIP is part of the cortical circuit that is specialized for 3D vision. Recent functional imaging studies of monkeys and humans support this notion. In monkeys, LOP, a region corresponding to CIP, was activated during the presentation of 3D shapes defined by texture gradient as well as motion parallax (24). In humans, the caudal intraparietal area, a human homolog of CIP, was activated when subjects attended to a 3D visual feature defined by texture gradients (25) and other kinds of depth cues (26, 27). However, it is uncertain how texture gradient signals are processed before they reach CIP. As for binocular disparity signals, neurons sensitive to absolute binocular disparity have been found in the monkey striate (4–7) and extrastriate (6–10) cortices. Particularly in V3, neurons were found to be in a columnar organization based on absolute binocular disparity (9). Because an anatomical study suggested that CIP receives fiber projections from V3 and V3A (28), CIP may depend on these areas for input of binocular disparity information.

References and Notes

1. K. N. Ogle, *Binocular Vision* (Hanfer, New York, 1964).
2. B. Julesz, *Foundation of Cyclopean Perception* (Univ. of Chicago Press, Chicago, 1971).
3. I. P. Howard, B. J. Rogers, *Binocular Vision and Stereopsis* (Oxford Univ. Press, New York, 1995).

4. H. B. Barlow, C. Blakemore, J. D. Pettigrew, *J. Physiol. (London)* **193**, 327 (1967).
5. T. Nikara, P. O. Bishop, J. D. Pettigrew, *Exp. Brain Res.* **6**, 353 (1968).
6. G. F. Poggio, B. C. Motter, S. Squatrito, Y. Trotter, *Vision Res.* **25**, 397 (1985).
7. G. F. Poggio, F. Gonzalez, F. Krause, *J. Neurosci.* **8**, 4531 (1988).
8. D. H. Hubel, M. S. Livingstone, *J. Neurosci.* **7**, 3378 (1987).
9. D. L. Adams, S. Zeki, *J. Neurophysiol.* **86**, 2195 (2001).
10. D. A. Hinkle, C. E. Connor, *Nature Neurosci.* **5**, 665 (2002).
11. M. Taira, K. I. Tsutsui, M. Jiang, K. Yara, H. Sakata, *J. Neurophysiol.* **83**, 3140 (2000).
12. K. I. Tsutsui, M. Jiang, K. Yara, H. Sakata, M. Taira, *J. Neurophysiol.* **86**, 2856 (2001).
13. T. Uka, H. Tanaka, K. Yoshiyama, M. Kato, I. Fujita, *J. Neurophysiol.* **84**, 120 (2000).
14. P. Janssen, R. Vogels, G. A. Orban, *Neuron* **27**, 385 (2000).
15. J. J. Gibson, *Perception of the Visual World* (Houghton Mifflin, Boston, 1950).
16. J. E. Cutting, R. T. Millard, *J. Exp. Psychol. Genet.* **113**, 198 (1984).
17. K. A. Stevens, *Biol. Cybern.* **42**, 95 (1981).
18. Gallant *et al.* (29) reported that several V4 neurons responded selectively to texture gradients. However, their involvement in depth perception appeared unlikely because the activity was more influenced by 2D retinal orientation than by 3D orientation.
19. Materials and methods are available as supporting material on Science Online.
20. E. Shikata, Y. Tanaka, H. Nakamura, M. Taira, H. Sakata, *Neuroreport* **7**, 2389 (1996).
21. In a previous study in CIP (12), we found some neurons to be sensitive to a monocular cue of linear perspective in addition to binocular disparity, although its effect was weaker than the effect of binocular disparity.
22. Activities of another example of texture gradient-selective neurons are shown in fig. S1.
23. It is possible that a high proportion of texture gradient-sensitive neurons were due to training of texture gradient discrimination before unit recording. However, we consider that the existence of texture gradient-sensitive neurons is not entirely a training effect and that those neurons normally exist in CIP. In a previous study by our group (20), in which no discrimination was required, many CIP neurons showed selectivity to a 3D surface orientation.
24. M. E. Sereno, T. Trinath, M. Augath, N. K. Logothetis, *Neuron* **33**, 635 (2002).
25. E. Shikata *et al.*, *J. Neurophysiol.* **85**, 1309 (2001).
26. M. Taira, I. Nose, K. Inoue, K. Tsutsui, *Neuroimage* **14**, 959 (2001).
27. B. Gulyas, P. E. Roland, *Proc. Natl. Acad. Sci. U.S.A.* **91**, 1239 (1994).
28. D. L. Adams, thesis, University College London (1997).
29. J. L. Gallant, D. C. van Essen, H. C. Nothdurft, in *Early Vision and Beyond*, T. V. Pappathomas, C. Chubb, A. Gorea, E. Kowler, Eds. (MIT Press, Cambridge, MA, 1995), pp. 89–98.
30. We thank Solidray Co. for assistance in developing computer programs for 3D graphics presentation. Supported by special coordination funds for promoting science and technology, a grant to promote multidisciplinary research projects, a grant-in-aid for scientific research on priority areas ("Advanced Brain Science Project" 14017085), a grant-in-aid for scientific research (13680903), and a grant-in-aid for JSPS Fellows (199900008) from the Ministry of Education, Culture, Sports, Science and Technology, Japanese Government.

Supporting Online Material

www.sciencemag.org/cgi/content/full/298/5592/409/DC1
Materials and Methods
Fig. S1

20 May 2002; accepted 30 July 2002

SUPPORTING ONLINE MATERIAL

Neural Correlates for Perception of 3D Surface Orientation From Texture Gradient

Ken-Ichiro Tsutsui¹, Hideo Sakata^{1,3}, Tomoka Naganuma^{1,2}, and Masato Taira¹

¹Department of Physiology and ²Department of Neurology, Nihon University School of Medicine, Tokyo 173-8610, Japan; and ³Laboratory for Anatomy and Physiology, Seitoku Junior College of Nutrition, Tokyo 124-8530, Japan

Correspondence should be addressed to: masato@med.nihon-u.ac.jp

Present address of Ken-Ichiro Tsutsui: Department of Anatomy, University of Cambridge, Cambridge CB2 3DY, United Kingdom

Material and methods

Two male Japanese monkeys (*Macaca Fuscata*) were used as subjects (monkeys #1 and 2) of this study. Throughout the experiments, the monkeys were treated in accordance with the NIH Guide for Care and Use of Laboratory Animals. The apparatus, techniques for single-unit recording and eye movement monitoring, and the procedure for neuronal data analysis were the same as those described previously (S1). For stimulus presentations, a stereoscopic display with a liquid-crystal polarized filter was used. All stimuli were depicted in red and black, and were presented through a circular window (35° in diameter) attached to the display.

Stimulus

Stimulus sets of texture pattern (TP) with dot elements (dot-TP, Fig. 1B) and random-dot stereogram (RDS) were used for two monkeys, and an additional stimulus set of texture pattern with line elements (line-TP) was used for monkey #2. Stimulus sets of TP were presented dichoptically on a stereoscopic display, but without any binocular disparity. Each stimulus set consisted of nine orientations, a surface in a frontoparallel plane and surfaces in eight different orientations that were slanted 45° against the frontoparallel plane and rotated every 45° around the sagittal axis. We used Stevens' (S2) definition of the direction of slant as "tilt", so that the tilt of the slanted plate ranged from 0 to 315° at 45° intervals. Monkeys were initially trained to perform a delayed-match-to-sample task of 3D surface orientation with dot-TP, RDS (monkeys #1 and 2), and

line-TP (monkey #2). After completion of the training, monkeys served as subjects of single-unit recording experiments lasting for approximately 6 months. During the single-unit recording, each stimulus set was used in a blocked manner. Each block usually consisted of 45 trials. As an additional stimulus set, a dot-TP was presented with binocular disparity so that the surface orientation defined by texture and disparity gradients would correspond. A stimulus set of line-TP was never presented with disparity.

Single unit recording and off-line data analysis

In this study, neuronal responses to the sample stimulus in successful trials only were analyzed. To examine whether a neuron was visually responsive, activities during 500-ms pre-stimulus and stimulus presentation periods were compared using Student's t-test ($p < 0.05$) for each orientation. If the result of t-test was significant at least in one orientation, the neuron was determined to be visually responsive. For a visually responsive neuron, selectivity to surface orientation was tested by comparing the responses to eight orientations, excluding frontoparallel orientation, using the Rayleigh test (S3).

The response frequencies for eight different orientations were converted into vectors ($\vec{r}_{0,1...7}$ for 0, 45... 315° tilt) so that the vector angle corresponded to the surface tilt and the vector length corresponded to the response frequency. The preferred orientation (tilt) was obtained by calculating the direction of the sum vector ($\sum \vec{r}$). For the index of the tuning sharpness, we used the angular

deviation S , which is equivalent to the standard deviation in linear statistics. The angular deviation S was calculated using

$$R = \left| \frac{\sum \vec{r}}{\sum |\vec{r}|} \right| \quad \text{and}$$

$$S = (180/\pi) [2(1-R)]^{1/2}$$

where $|\sum \vec{r}|$ is the length of the sum vector, $\sum |\vec{r}|$ is the sum length of each vector, and S is the angular deviation in degrees.

Responses to nine orientations of each stimulus set were averaged across selective neurons with the strongest response re-aligned as 0° tilt (Fig. 3). Gaussian curve was fitted to the data by chi-square method, according to following equation:

$$f(x_i) = a \exp\{-0.5(x_i/\sigma)^2\} + b$$

where $f(x_i)$ is discharge frequency with surface tilt x_i , b is baseline response (average of responses to the orientation which is diagonal to the preferred orientation and responses to orientations which are adjacent to the diagonal orientation), and a and σ as regression coefficients.

Behavioral test of TP-RDS cross matching

After the single unit recording, behavioral test was attempted to confirm that monkeys perceive depth from texture gradient. Monkeys were trained to cross-match the surface orientations defined by texture and disparity gradients using TPs without any disparity as sample stimuli and RDSs as test stimuli. To perform this cross-matching correctly, monkeys had to ignore the 2D

features of TPs and RDSs, and attend to the 3D surface orientation defined by texture gradient and disparity gradient. As we had expected, the monkeys initially could not perform the task correctly. Almost all of their mistakes at that time were judging ‘different’ when the orientations defined by TP and RDS were ‘the same’, suggesting that the monkeys were performing the discrimination based on the 2D features of stimuli. Therefore, we intended to make monkeys learn the rule of the task using only diagonal orientations of TP with dot elements (dot-TP) and RDS (rule learning session), and see whether this learning is transferred to the cross-matching of oblique orientations of dot-TP and RDS (test session). Only in the initial stage of the learning session with monkey #1, disparity was added to dot-TPs in order to facilitate learning (data not shown). After the monkeys attained constant >80% success rates, the test session was started. The monkeys were tested with oblique orientations of dot-TP and RDS (Test 1). For monkey #2, cross-matching of diagonal and oblique orientations of TP with line elements (line-TP) and RDS was also required as test sessions (diagonal: Test 2, oblique: Test 3). In the initial block of each test session, all trials including error trials were rewarded, in order to examine monkeys’ performance without correct/error feed back. In the following blocks, only success trials were rewarded as ordinary blocks.

Supporting figure

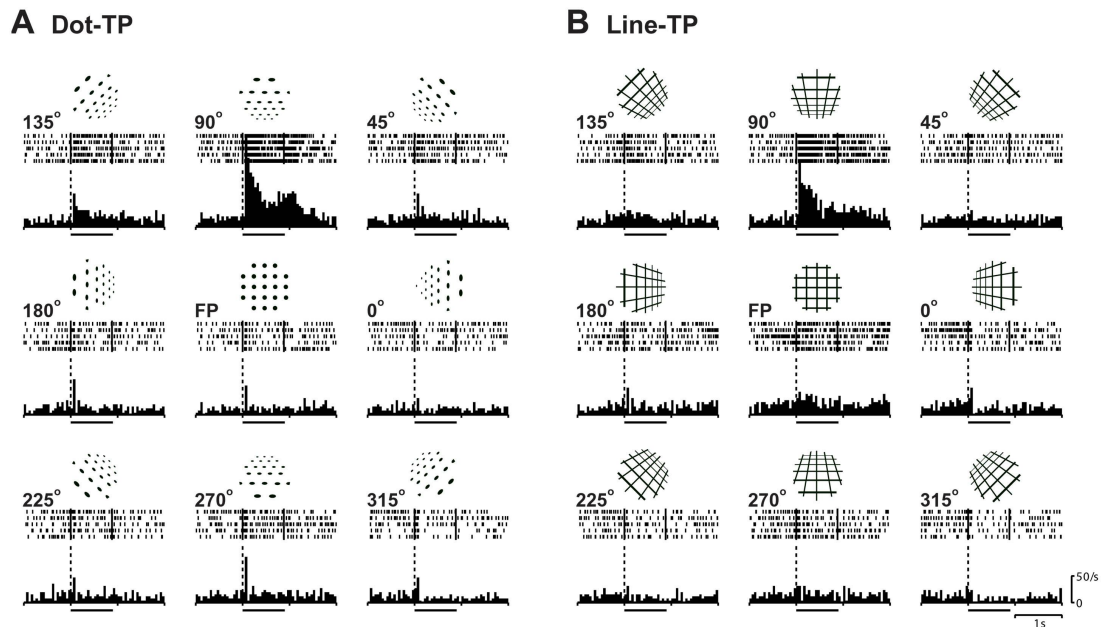


Fig. S1. Activities of a texture-gradient selective neuron. Responses to nine orientations of dot-TP (A) and line-TP (B) are shown. Bars below histograms indicate stimulus presentation duration. Insets above rasters indicate the stimuli presented. Numbers at the top left of the rasters indicate tilt angle in degree. FP indicates the frontoparallel orientation. This neuron showed selective response to the texture gradient of forward tilt (90° tilt), regardless of the difference of texture pattern.

Supporting references and notes

- S1. K. I. Tsutsui, M. Jiang, K. Yara, H. Sakata, M. Taira, *J. Neurophysiol.* **86**, 2856 (2001)
- S2. K. A. Stevens, *Percept. Psychophys.* **33**, 241 (1983)
- S3. K. V. Mardia, *Statistics of Circular Data*, Academic, New York (1972)

unique shape and orientation, are all essential components for understanding tooth formation in these worms.

The discovery of magnetite in the teeth of chitons initiated a series of investigations that contributed significantly to our understanding of basic processes of biomineralization. The discovery of this copper chloride mineral in the teeth of another invertebrate may well do the same. There is

still much to learn about the mechanisms involved in controlled mineral formation.

References and Notes

1. H. A. Lowenstam, *Bull. Geol. Soc. Am.* **73**, 435 (1962).
2. H. C. Lichtenegger *et al.*, *Science* **298**, 389 (2002).
3. A hydrated copper oxalate, moolooite, is formed by certain lichens growing on copper-bearing rocks. The mineral is formed by the reaction between oxalic acid secreted by the lichen and the rock, and its formation is presumably poorly controlled (8).
4. G. W. Bryan, P. E. Gibbs, *J. Mar. Biol. Assoc. U.K.* **59**, 969 (1979).

5. J. E. Hillerton, J. F. V. Vincent, *J. Exp. Biol.* **101**, 333 (1982).
6. M. Voss-Foucart, M. Fonze-Vignaux, C. Jeuniaux, *Biochem. Syst. Ecol.* **1**, 119 (1973).
7. S. Weiner, H. D. Wagner, *Annu. Rev. Mat. Res.* **28**, 271 (1998).
8. J. E. Chisholm, G. C. Jones, O. W. Purvis, *Min. Mag.* **51**, 715 (1987).
9. H. A. Lowenstam, S. Weiner, *On Biomineralization* (Oxford Univ. Press, New York, 1989).

Supporting Online Material

www.sciencemag.org/cgi/content/full/298/5592/375/DC1 Table S1

PERSPECTIVES: NEUROSCIENCE

Reconstructing a 3D World

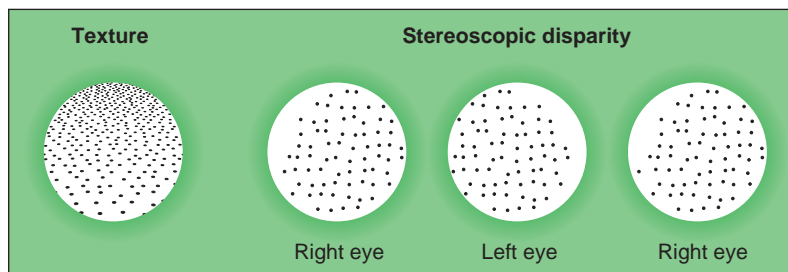
Charles E. Connor

Information in the visual system starts out as a two-dimensional (2D) pattern of neural activity across the retina. Yet the world we perceive is three-dimensional (3D). The neural mechanisms for reconstructing this 3D reality from 2D sensory inputs have long fascinated scientists. Much research has focused on stereopsis—inferring depth position from small image disparities between the right and left eyes. Neurons in the primary visual cortex (V1), V2, and many other visual areas are sensitive to such disparities, providing the signals that enable us to perceive depth stereoscopically (1–3). However, even without stereopsis—for example, when viewing photographs or movies—we still obtain vivid impressions of depth. This kind of nonstereoscopic 3D perception depends on other cues such as shading, perspective, texture gradients, and motion parallax. Two articles in this issue, one by Tsutsui *et al.* on page 409 (4) and one by Vanduffel *et al.* on page 413 (5), break new ground in understanding how the brain uses such cues to infer 3D structure.

Tsutsui and colleagues (4) used electrophysiological recording to study responses of single neurons in the caudal intraparietal sulcus (CIP) of the monkey brain. CIP is part of the dorsal visual pathway, which processes large-scale spatial information. This group has already shown that CIP neurons are tuned for 3D

surface orientation defined by stereoscopic disparity and perspective cues (6, 7). Here, they report that CIP neurons are also sensitive to texture-based depth cues. Texture gradients convey 3D orientation through gradual changes in the size, shape, and spacing of small surface elements (see the figure).

One striking aspect of the Tsutsui *et al.* results is that most cells showed identical tuning for surfaces defined by texture gra-



Making 3D a reality. The figure shows how texture and stereopsis suggest the same surface orientation in different ways. (Left) The gradual bottom-to-top decrease in texture element size and spacing implies that the surface is slanting away toward the top. (Right) A random dot stereogram, with no changes in texture size or spacing, but with a bottom-to-top gradient in dot position disparity (between the right and left eye images). Readers can either uncross their eyes to view the right pair of circles or cross their eyes to view the left pair. This stereogram produces the same percept of surface slant.

dients and for surfaces defined by purely stereoscopic cues. The figure shows how texture and stereopsis suggest the same surface orientation in different ways. The majority of CIP neurons tested with both of these very different cues showed consistent selectivity for the same surface orientations. Such convergence of coherent information from different sources is unlikely to occur by chance. Thus, these investigators provide unusually strong evidence for CIP's involvement in 3D surface perception.

3D surface orientation tuning has also been demonstrated in region MT/V5, another dorsal visual pathway area, using random dot stimuli with stereoscopic disparity (8) and motion parallax (9) cues. In contrast, many

neurons in area V4, part of the object-related ventral visual pathway, are tuned for the 3D orientation of elongated stimuli (rectangular bars) but not continuous surfaces (10). It may be that the dorsal (spatial) pathway is specialized for representing 3D surfaces, which can pertain to objects but can also define the large-scale spatial structure of landscapes and buildings. (The ground, for example, usually slants away from the viewer in the direction shown in the figure.) The ventral (object) pathway may be more concerned with 3D contours (edges and lines), which contain the most information about object shape.

The importance of electrophysiological studies in monkeys, exemplified by the Tsutsui *et al.* work, lies partly in their implications for human vision. Monkeys have long been considered a good model for human vision because of their similar visual capacities and evolutionary proximity. The relationship has turned out to be even closer, as shown by functional magnetic resonance imaging (fMRI) studies of visually evoked neural activity in humans. These studies reveal a similar arrangement of retinotopic maps (that is, retinal maps of visual space) and specialized responses across the surface

of the visual cortex in the two species. As a result, there is a strong case for homology between monkey and human areas V1, V2, V3, V3A, VP, V4v (ventral V4), and MT/V5 (11, 12). Thus, it is now possible to study detailed neural mechanisms in the monkey and point to specific areas of the human brain where the same processing may occur.

Such cross-species comparisons usually rely on electrophysiology in monkeys and fMRI in humans. Vanduffel and colleagues, in their study of motion-based 3D perception (5), have taken the more direct approach of using fMRI on awake subjects of both species. This has the obvious advantage of closer technical equivalence between experiments. It also overcomes the

The author is in the Department of Neuroscience and the Zanvyl Krieger Mind/Brain Institute, Johns Hopkins University, Baltimore, MD 21218, USA. E-mail: connor@jhu.edu

data limitations of monkey electrophysiology, which is ideal for examining circuit-level information processing but slow and indirect for measuring neuronal population activity in multiple brain areas. Vanduffel *et al.* used this parallel fMRI approach to show that organization of motion-based 3D processing in monkeys and humans is partly analogous, but also has some striking dissimilarities that may reflect functional differences in higher level visual areas.

The stimuli used by Vanduffel *et al.* were “bent paper clip” figures undergoing rotation in depth, which produces 2D image transformations that convey 3D shape (13) [see their online movie (5) or reproduce the phenomenon yourself by twirling a bent paper clip and observing its shadow]. The control stimuli were the same bent paper clip figures translating back and forth across the image plane. The contrast between fMRI responses to 3D rotation and 2D translation was used to identify brain regions sensitive to 3D shape-from-motion.

Vanduffel and colleagues report that several areas are sensitive to 3D shape-from-motion in both species: V2, V3, and MT/V5, all of which are known to process motion and depth information. In the monkey, FST (fundus of the superior temporal sulcus) and V4 also responded preferentially to 3D stimuli. Area FST has no identified homolog in humans. Human V4 has been partially identified: The ventral portion (V4v), representing the upper visual field, has been localized with retinotopic mapping (11, 12). Human V4v does not appear to have been differentially activated in this study. The expected location for dorsal human V4 (V4d) would be posterior to MT/V5, although retinotopic mapping suggests that no V4d homolog exists in this location (14). This area (labeled LOS by Vanduffel *et al.*) did respond preferentially to motion-based 3D shape. Previous fMRI studies have shown that this region is also sensitive to motion-defined boundaries (14–16).

The most striking interspecies differences were found in the intraparietal sulcus (IPS). There were four distinct foci in human intraparietal cortex. These corresponded to previously identified regions sensitive to motion and shape-from-motion (17, 18). In the monkey, no differential activity was observed in IPS. The homology between human and monkey parietal areas is uncertain, but the complete lack of activity in monkey IPS suggests a strong species difference.

In contrast with these results, a previous study in anesthetized monkeys by Sereno and colleagues (19) revealed several foci in the IPS with preferential responses to motion-based (and texture-

based) 3D shape. Sereno *et al.* also found activity in middle and anterior STS (superior temporal sulcus), which Vanduffel *et al.* did not. On the other hand, Vanduffel *et al.* found activity in V4, whereas Sereno *et al.* did not. Some of these discrepancies could reflect different significance criteria. There are certainly differences between anesthetized and awake visual responses, but one would expect higher level visual areas in IPS and STS to be less sensitive rather than more sensitive to 3D structure under anesthesia. The most likely cause for the widely discrepant activation patterns is stimulus differences. Sereno *et al.*'s shapes were composed of surfaces (defined by moving dots), which may be more effective stimuli for dorsal pathway areas in IPS and STS (upper bank) as discussed above. Vanduffel *et al.* presented their subjects with bent paper clip stimuli composed of 3D-oriented limbs, which may be more effective for stimulating ventral pathway areas like V4 (10).

More surprising are the discrepancies between these two fMRI studies and a number of electrophysiological studies, including those by Tsutsui *et al.* There is now electrophysiological evidence for 3D surface orientation tuning in CIP (4, 6, 7) (based on stereoscopic, texture gradient, and perspective cues) and in MT/V5 (8, 9) (based on stereoscopic and motion parallax cues). There is also evidence for 3D bar orientation tuning in V4 (10) (stereoscopic cues) and 3D shape tuning in IT (inferotemporal) cortex (20, 21) (stereoscopic cues). MT/V5 has also been specifically implicated in 3D shape-from-motion processing (22). One might predict that all of these areas would be differentially sensitive to 2D versus 3D shapes, but only MT/V5 gave a positive result in both fMRI experiments. The inconsistencies could be due to depth cue differences—the fMRI studies were based on motion, whereas the electrophysiological studies were based on stereoscopic disparity, texture gradients, and perspective. However, one would expect that visual areas processing 3D structure would, like CIP, take advantage of multiple cues (4, 6, 7).

The more general explanation for these discrepancies may be that information processing at the local circuit level does not necessarily correlate with neuronal population activity measured by fMRI. Electrophysiology strongly indicates 3D processing in CIP (4, 6, 7) and IT cortex (20, 21), but this need not entail enhanced population-level responses to 3D stimuli. If positive and negative response changes at the local level balance out on a larger scale, CIP and IT cortex would exhibit equiva-

lent overall responses to 2D and 3D stimuli, as observed by Vanduffel and co-workers.

Conversely, differential population activity does not necessarily imply any specific kind of information processing—preference for 3D stimuli does not have to signify tuning for 3D structure. A given area may represent non-3D information but still respond best to 3D stimuli, perhaps because they are more complex, coherent, realistic, or object-like. Conclusions about 3D processing depend on careful controls (Vanduffel *et al.* specifically controlled for the effects of 2D rotation and expansion/contraction; Sereno *et al.* controlled for local motion coherence and 2D boundary shape differences) and electrophysiological confirmation at the local circuit level.

All of this highlights the need for an evolving interplay between large-scale imaging studies (like that of Vanduffel *et al.*) and fine-scale analysis of neural mechanisms (like that of Tsutsui *et al.*). Imaging techniques can be used to assess whole-brain activity, and they provide the critical link between monkey and human vision. Electrophysiology addresses circuit-level information processing and remains important for interpreting the population-level differences revealed by fMRI. Every imaging result poses questions for a future electrophysiological experiment, and vice versa. Imaging and electrophysiological experiments with equivalent stimuli and perceptual conditions will be required to fully elucidate how the brain constructs a 3D reality from its 2D sensory inputs.

References

1. H. B. Barlow *et al.*, *J. Physiol. (London)* **193**, 327 (1967).
2. D. H. Hubel, T. N. Wiesel, *Nature* **225**, 41 (1970).
3. G. F. Poggio, B. Fischer, *J. Neurophysiol.* **40**, 1392 (1977).
4. K.-I. Tsutsui *et al.*, *Science* **298**, 409 (2002).
5. W. Vanduffel *et al.*, *Science* **298**, 413 (2002).
6. E. Shikata *et al.*, *Neuroreport* **7**, 2389 (1996).
7. K. Tsutsui *et al.*, *J. Neurophysiol.* **86**, 2856 (2001).
8. J. D. Nguyenkim, G. C. DeAngelis, *Soc. Neurosci. Abstr.* **27**, (2001).
9. D. K. Xiao *et al.*, *Eur. J. Neurosci.* **9**, 956 (1997).
10. D. A. Hinkle, C. E. Connor, *Nature Neurosci.* **5**, 665 (2002).
11. E. A. DeYoe *et al.*, *Proc. Natl. Acad. Sci. U.S.A.* **93**, 2382 (1996).
12. M. I. Sereno *et al.*, *Science* **268**, 889 (1995).
13. H. Wallach, D. N. O'Connell, *J. Exp. Psychol.* **45**, 205 (1953).
14. R. B. Tootell, N. Hadjikhani, *Cereb. Cortex* **11**, 298 (2001).
15. G. A. Orban *et al.*, *Proc. Natl. Acad. Sci. U.S.A.* **92**, 993 (1995).
16. S. Van Oostende *et al.*, *Cereb. Cortex* **7**, 690 (1997).
17. G. A. Orban *et al.*, *Neuron* **24**, 929 (1999).
18. S. Sunaert *et al.*, *Exp. Brain Res.* **127**, 355 (1999).
19. M. E. Sereno *et al.*, *Neuron* **33**, 635 (2002).
20. P. Janssen *et al.*, *Proc. Natl. Acad. Sci. U.S.A.* **96**, 8217 (1999).
21. P. Janssen *et al.*, *Science* **288**, 2054 (2000).
22. D. C. Bradley *et al.*, *Nature* **392**, 714 (1998).